ELSEVIER

Science and Technology of Advanced Materials 2 (2001) 117–126

SCIENCE AND TECHNOLOGY OF ADVANCED MATERIALS

www.elsevier.com/locate/stam

Microstructure evolution in equiaxed dendritic growth

C. Beckermann*, Q. Li, X. Tong

Department of Mechanical Engineering, The University of Iowa, Iowa City, IA 52242, USA

Abstract

Microstructure evolution in equiaxed dendritic solidification is investigated through the study of free dendritic growth in a supercooled melt. A detailed measurement of microstructural features (such as side-branch spacings, envelope shape, projection area, and contour length) of freely growing succinonitrile dendrites is performed using images from the microgravity experiment of Glicksman and co-workers. The measurements show that the microstructure evolution of an equiaxed dendrite is divided into two regimes: an initial linear regime and a subsequent non-linear coarsening regime. It is found that unique scaling relations exist between the measured geometry parameters and the primary tip radius or speed for both regimes. The underlying mechanisms involved in dendritic structure evolution are discussed. In addition, using the phase-field method, we perform numerical experiments to investigate the effects of melt convection on equiaxed dendritic growth. The dendrite tip operating state (i.e. the tip velocity and radius) is quantitatively evaluated as a function of the flow velocity and dendrite orientations and compared with Microscopic Solvability Theory. Other structural features (such as the side-branches) of an equiaxed dendrite in the presence of flow are also examined in order to show how convection influences microstructure evolution in equiaxed dendritic growth.

Keywords: Equiaxed dendrite; Dendritic growth; Microstructure; Phase field; Convection

1. Introduction

Equiaxed dendritic solidification or free dendritic growth is a frequently observed growth mode in casting and welding processes. The understanding and control of its structures are therefore of great importance to metallurgical engineers. Due to its rich behavior as a non-linear phase transformation process, equiaxed dendritic growth has also drawn much research attention in physics and mathematics communities.

Three different stages can be distinguished in free dendritic growth: (i) the steady-state propagation of the tip region; (ii) the linear, nearly periodic formation of the initial side-branches; and (iii) the non-linear, irregular side-branching evolution. The tip is the best-studied region of the dendrite. Many theoretical, numerical and experimental efforts have been devoted to investigate the steady-state growth of the tip region, and they have resulted in enormous advances in the understanding of this phenomenon [1–5]. In this paper the focus is on: (i) the microstructural evolution in the side-branching region away from the tip; and (ii) the influence of convection on dendritic growth.

The formation of dendritic side-branches can generally be attributed to the Mullins–Sekerka instability [6]. Based on this idea, Langer and co-workers [7–9] investigated the thermal noise amplification mechanism for side-branching, which has become the preferred explanation for the side-branching phenomenon. However, a comparison between Langer's three-dimensional symmetric model [8] and the experimental results of Huang and Glicksman [4] shows only approximate, qualitative agreement and the experimentally observed side-branches have much larger amplitudes than can be explained by purely thermal noise in the model. This discrepancy was ascribed later by Brener and Temkin [10] to the assumption of a paraboloidal needle crystal in Langer's model. Brener and Temkin's model [10], which is based on the more realistic non-axisymmetric, three-dimensional needle-crystal shape proposed by Brener [11], indeed predicts much faster-growing side-branch amplitudes than Langer's symmetric model. The predicted side-branch amplitudes are also found to be in reasonable agreement with the experimental results of Bisang and Bilgram [12,13] for xenon dendrites and with the experimental results of La Combe et al. [14] for succinonitrile (SCN) dendrites [13]. These studies confirm that the side-branches are indeed triggered by thermal noise. However, available measurements of the initial side-branch spacing are not well predicted by either Langer's model or Brener and Temkin's model.

The above-mentioned models only deal with the initial, linear side-branching behavior. For the region further

* Corresponding author. Tel.: +1-319-335-5681; fax: +1-319-335-5669.
E-mail address: becker@icaen.uiowa.edu (C. Beckermann).

1468-6996/01/$ - see front matter
PII: S1468-6996(01)00037-7

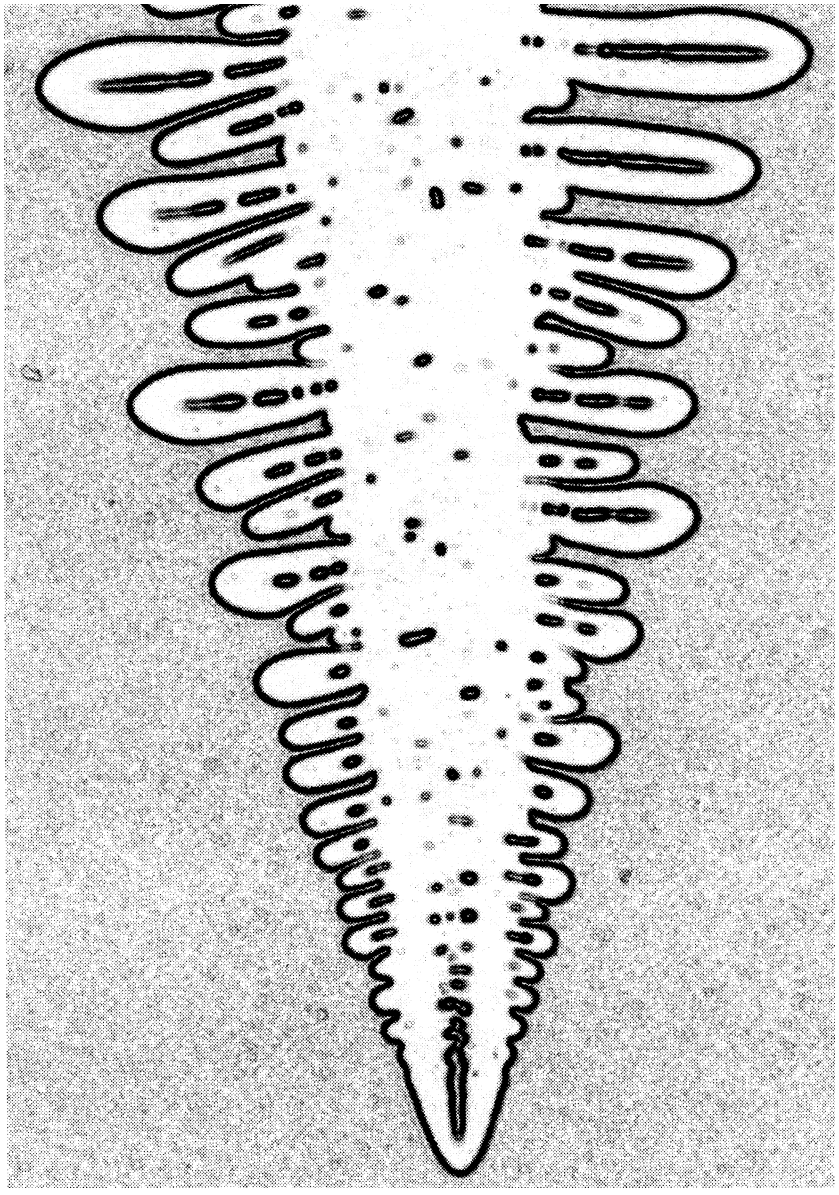

Fig. 1. Example of a side-branching dendrite growing into a supercooled melt: the image is from the microgravity experiment of Glicksman and co-workers [5] for SCN.

away from the tip (i.e. the non-linear side-branching regime), no theories are available to describe its strongly non-linear coarsening behavior. Brener and Temkin's model, [10] accounts for the competitive growth of active or survived side-branches only. Experiments by Hürlimann et al. [15] using xenon and Dougherty and Chen [16] using an NH_4Cl solution, as well as the measurements of Li and Beckermann [17] on SCN dendrites, have demonstrated that the side-branch structure far from the tip is still self-similar and can be scaled with the tip radius R. These experimental findings agree well with Brener and Temkin's prediction [10] that this strongly non-linear growth regime is self-similar up to $Z/R \ll 1/Pe$, where Z is the distance from the tip and Pe is the tip Peclet number. However, many of the experimental findings have not yet been explained theoretically and can only be treated as empirical results.

In parallel with theoretical and experimental advances in understanding microstructural evolution in free dendritic growth, significant progress in numerical modeling has recently been made due to the advent of the phase-field method [18–20]. The phase-field approach belongs to a larger class of methods that rely on treating a microscopically sharp interface as a diffuse region immersed in the calculation domain. Its attractiveness is rooted in the fact that explicit tracking of the interface and explicitly satisfying interfacial boundary conditions are completely avoided by solving a certain evolution equation for the phase-field variable. This makes it especially suitable for simulating the formation of complex interfacial patterns in solidification.

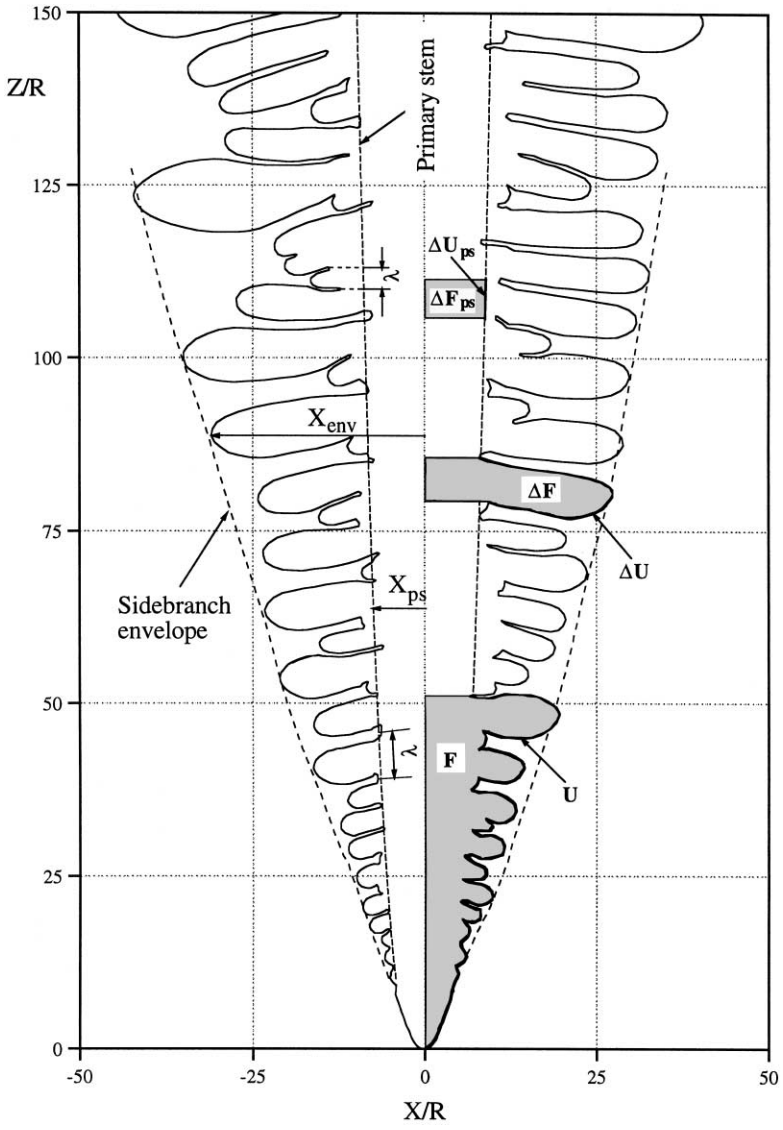

Fig. 2. Schematic illustration of the measurements performed in the present investigation.

Indeed, using the phase-field method several investigators (see Ref. [21] and the references therein) have succeeded in simulating the morphological evolution of 2D and 3D dendrites with side-branches, something that is difficult to achieve using conventional front-tracking methods. So far most phase-field simulations are limited to diffusion-controlled growth at relatively large dimensionless supercoolings.

In this paper, the authors review their recent results in understanding and modeling the morphological evolution of an equiaxed dendrite. The work involves both measurements of the structure of freely grown SCN dendrites using images from the microgravity experiments of Glicksman et al. [5] and phase-field simulations of equiaxed dendritic solidification with convection. The experimental study focuses on microstructural evolution in the side-branching regime, and the underlying mechanisms involved in the side-branching structure development are discussed. With respect to numerical modeling, the phase-field method is employed to investigate the influence of melt convection on microstructural evolution in equiaxed dendritic growth. The emphasis is on the quantitative evaluation of the dendrite tip operating state (i.e. the tip velocity and radius) and the initial side-branching behavior.

2. Measurements of dendrite morphology

A typical freely growing dendrite branch is shown in Fig. 1. The image is from the microgravity experiment of Glicksman and co-workers [5] for SCN. The three different regimes mentioned in Section 1 can be easily identified in this image. In order to characterize the morphological features of a dendrite in the side-branching regimes, a number of measurable geometrical parameters are proposed: the envelope of the active or surviving side-branching tips,

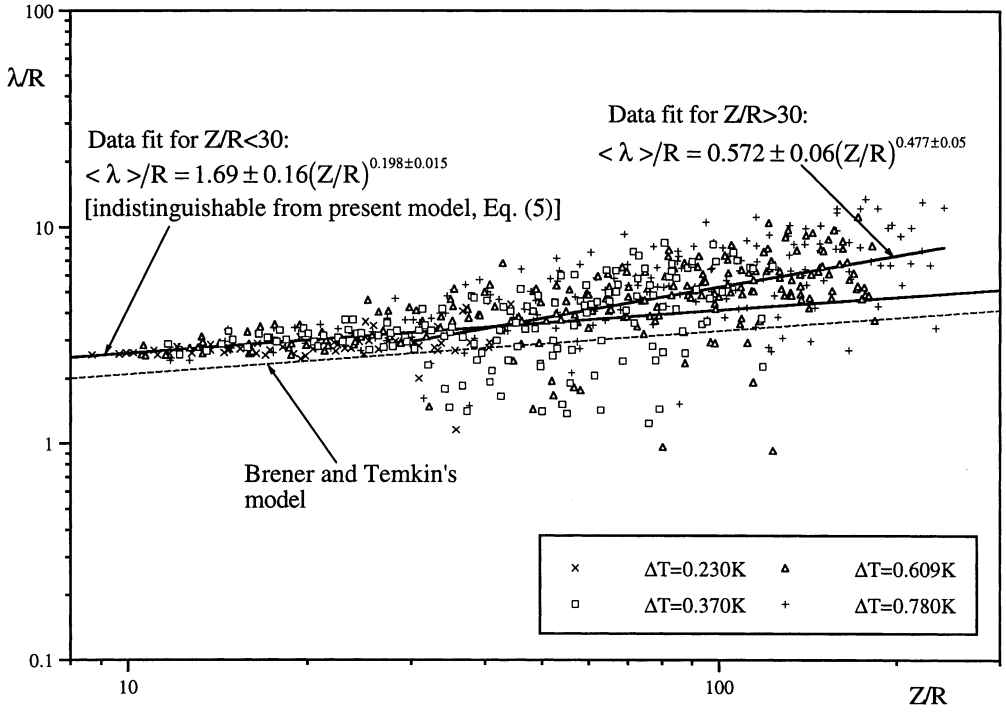

Fig. 3. Measured normalized secondary arm spacings (symbols), λ/R, as a function of the normalized distance, Z/R, from the primary tip; the two solid lines represent a best fit of the data for $Z/R < 30$ and $Z/R > 30$, respectively; the interrupted lines are model results for the initial linear side-branching regime (with $\sigma = 0.02$).

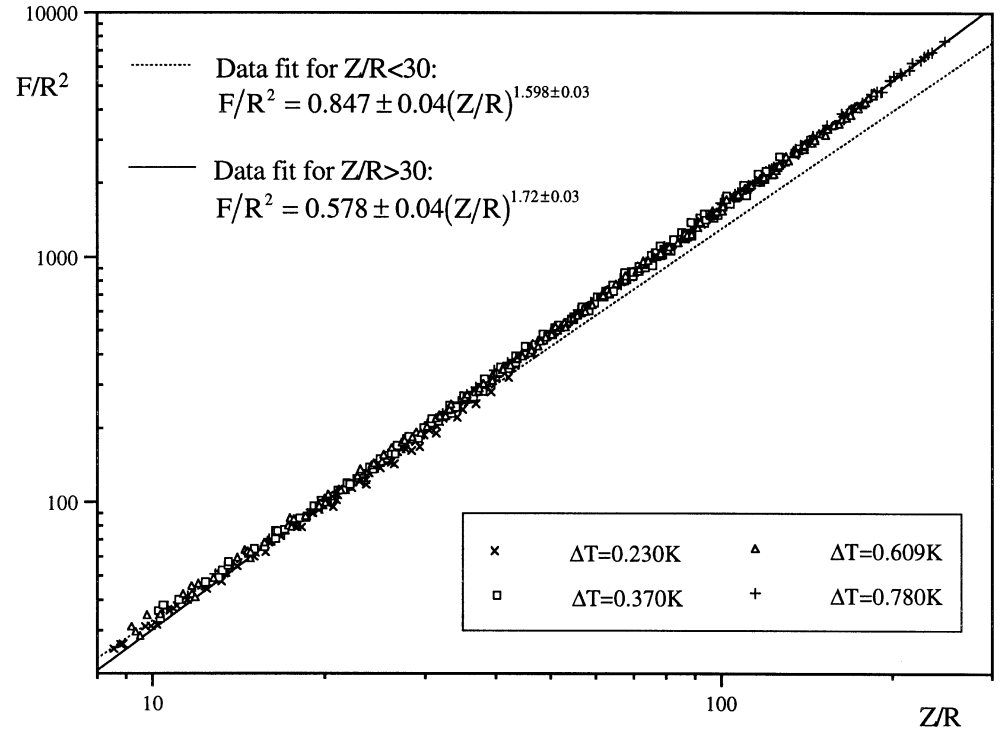

Fig. 4. Normalized projection area, F/R^2, versus normalized distance from the tip, Z/R; the two lines represent a best fit of the data for $Z/R < 30$ and $Z/R > 30$, respectively.

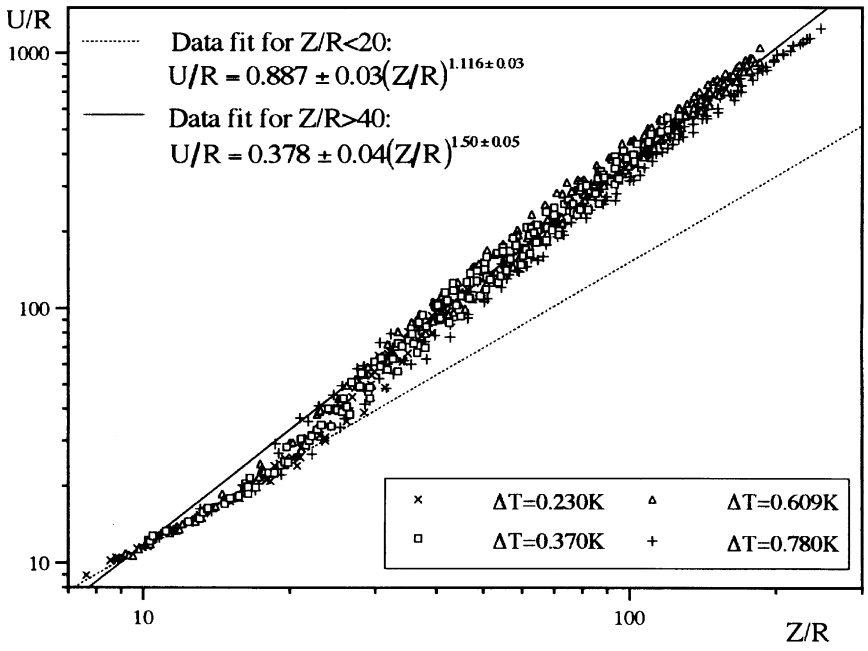

Fig. 5. Normalized contour length, U/R, versus normalized distance from the tip, Z/R; the two lines represent a best fit of the data for $Z/R < 20$ and $Z/R > 40$, respectively.

X_{env}; the side-branch spacings, λ, the contour length, U; and the area, F, of the projection of a dendrite, and the primary stem contour, X_{ps}. The definitions and the measurements of these geometrical parameters are illustrated schematically in Fig. 2. For other details, refer to Refs. [17,22].

The measurements are performed on images from the microgravity experiment of Glicksman et al. [5] for free dendritic growth of SCN into a uniformly supercooled melts. The supercoolings analyzed here vary from 0.23 to 0.78 K, which give tip radii ranging from 19 to 72 μm. Figs. 3–5 show the results of the side-branch spacing, projection area and contour length measurements, respectively, normalized by the tip radius, in log–log plots. The measurements clearly show that: (i) the dendrites are self-similar and can be scaled with the tip radius; and (ii) there exist two different regimes that are divided at about $Z/R = 30$. The two regimes correspond to the initial linear and the subsequent non-linear side-branching regimes and are discussed in Sections 2.1 and 2.2, respectively.

2.1. Initial linear side-branching regime

The initial side-branching regime of a dendrite is characterized by the growth of the first few branches newly formed near the dendrite tip. The measured side-branch spacings, projection area and contour length in this regime all fall into a narrow band in Figs. 3–5, respectively, demonstrating that the initial side-branch formation is a well-defined instability that can be scaled with the tip radius. A power-law fit of the measured spacing data for $Z/R < 30$ gives the variation of the average spacing $\langle\lambda\rangle$ with Z as:

$$\langle\lambda\rangle/R = (1.69 \pm 0.16)(Z/R)^{0.198\pm0.015}. \quad (1)$$

Using this result, the authors tested Brener and Temkin's non-axisymmetric model, which is based on the non-axisymmetric needle crystal shape and predicts the spacings as:

$$\lambda/R = 2\pi(3/5)^{3/10}\sqrt{3\sigma}(Z/R)^{1/5} \approx 1.32(Z/R)^{1/5}, \quad (2)$$

where σ is the usual selection constant [≈0.02 for SCN]. Although Brener and Temkin's model has previously shown good quantitative agreement in the side-branch amplitude with experimental measurements [13], its side-branch spacing prediction (Eq. (2)) agrees only qualitatively with the present measurements (Eq. (1)). There is a nearly 30% deviation that cannot be explained by measurement error. In order to overcome this shortcoming, the authors developed a simple model of the initial side-branch spacing development. The following is a brief description of this model. A more detailed discussion can be found in Ref. [22].

The present model is based on a Mullins–Sekerka instability analysis performed on the needle crystal surface. Mullins–Sekerka's linear stability analysis gives the local critical and maximum instability wavelengths, λ_c and λ_m, as:

$$\lambda_c = 2\pi\sqrt{2\alpha_l d_0/V_n} \quad \text{and}$$
$$\lambda_m = 2\pi\sqrt{6\alpha_l d_0/V_n} = \sqrt{3}\lambda_c, \quad (3)$$

where V_n is the local normal interfacial velocity, α_l is the thermal diffusivity of the liquid, and d_0 is the capillary length. For the non-axisymmetric 3D needle crystal shape of Brener [11], there is the following expression for V_n along the ridges:

$$V_n = V_t[1 + (\tfrac{5}{3}Z/R)^{4/5}]^{-1/2}, \quad (4)$$

where V_t is the dendrite tip velocity. Substituting Eq. (4) into Eqs. (3), and using the usual selection criterion for the dendrite tip operating state $\sigma = 2\alpha_l d_0/(V_t R^2)$, the variation of the local maximum instability wavelength λ_m with distance away from the primary tip, Z, for the non-axisymmetric needle crystal is given by:

$$\lambda_m/R = 2\pi\sqrt{3\sigma}\,[1 + (\tfrac{5}{3}Z/R)^{4/5}]^{1/4} \approx 1.72(Z/R)^{1/5}. \quad (5)$$

The approximate expression is a curve fit for $8 < Z/R < 30$ and an experimental value of $\sigma = 0.02$ for SCN [4]. Eq. (5) is identical in form to Eq. (2) from Brener and Temkin's model [10], except for the value of the pre-factor. The agreement with this more sophisticated model implies that the present model, despite its simplicity, is essentially correct.

The present arm spacing measurements, being made on dendrites grown in a convection-free environment, allow for a comparison with the model over the entire linear side-branching regime, which is shown in Fig. 3. Both the exponent of 0.198 ± 0.015 and the pre-factor of 1.69 ± 0.16 in the experimental correlation, Eq. (1), are in excellent agreement with the present model for the maximum instability wavelength of the non-axisymmetric needle crystal (Eq. (5)). This good agreement not only validates the present simple model but also confirms that: (i) the maximum, and not the critical, instability wavelength determines the observed initial side-branch spacing; and (ii) the non-axisymmetric needle crystal of Brener [11] gives a realistic dendrite shape. Furthermore, since the present model relies directly on the Mullins–Sekerka stability theory, the present comparison can be regarded as an experimental validation of this important theory.

While the selection mechanism of the initial side-branch spacings is well clarified by the present spacing measurement and model, the projection area measurement allows the demonstration of another important growth mechanism of dendritic crystals. The measured data for the projection area F for $Z/R < 30$ can be fitted by a power law which yields the following scaling relation:

$$F/R^2 = (0.847 \pm 0.04)(Z/R)^{1.598\pm0.03}. \quad (6)$$

Comparing with the behavior of $F(Z)$ for the non-axisymmetric needle crystal model of Brener [11], $F/R^2 \approx 0.85(Z/R)^{1/6}$, the present correlation of $F(Z)$ (Eq. (6)) shows the same scaling exponent of 1.6 and the same prefactor of 0.85 to within the measurement uncertainty. The fact that real dendrites with side-branches and a needle crystal (without side-branches) have the same projection area indicates that the theoretical steady-state solution is preserved in some geometrical parameters (the projection area here) of the actual dendritic pattern. Similar results have been reported by Counder et al. [23] for two-dimensional dendritic growth, anisotropic viscous fingering, and anisotropic diffusion-limited aggregation. While the projection area is exactly preserved in the initial linear regime, it can be seen from Fig. 4 that a small deviation of $F(Z)$ exists from that of the needle crystal in the non-linear regime. This deviation may be attributed to coarsening, which is discussed in Section 2.2.

2.2. Non-linear regime

As the side-branches evolve into a non-linear regime far down from the tip, a coarsening phenomenon occurs during which some side-branches continue to grow as others are squeezed out, resulting in a very irregular side-branch structure. It is presently not clear whether this coarsening process can be described by available theories. Hence, the purpose here is simply to define and measure meaningful geometrical parameters of side-branching dendrites in the non-linear coarsening regime, and to assess the need to develop new theories of coarsening of the side-branch structure in free dendritic growth.

The measurements of the side-branch envelope and the side-branch spacing are a preliminary attempt to understand the coarsening process of the side-branching structure in the non-linear regime. These measurements experimentally verify the coarsening mechanism due to the competitive growth of the active side-branches [17] and confirm that the coarsening of the structure near the junction between an arm and the primary stem is dominantly driven by the reduction of the interfacial free energy [22]. Unfortunately, the measurements only reveal two individual coarsening phenomena that occur at two special locations of a side-branching dendrite, respectively. In order to investigate the overall coarsening of a side-branching dendrite as a whole, 'integral' parameters have to be used. Such integral parameters take into account all of the non-linear interactions among the different side-branches.

There are two integral parameters that can be used to characterize the overall properties of a dendrite: the volume and the surface area of a dendrite. Since direct measurement of these two parameters during growth is not possible, instead the measured projection area F and the contour length U of a dendrite in the side-branch plane are used. Fitting the measured data in Figs. 4 and 5 yields:

$$F/R^2 = (0.578 \pm 0.04)(Z/R)^{1.72\pm0.003} \quad \text{for } Z/R > 30, \quad (7)$$

$$U/R = (0.378 \pm 0.04)(Z/R)^{1.50\pm0.05} \quad \text{for } Z/R > 40. \quad (8)$$

An important geometrical parameter that can be derived directly from the measurement of F and U is the dimensionless parameter $\mathrm{d}F/(R\mathrm{d}U)$. This represents a local mean characteristic length that can be used to describe the overall

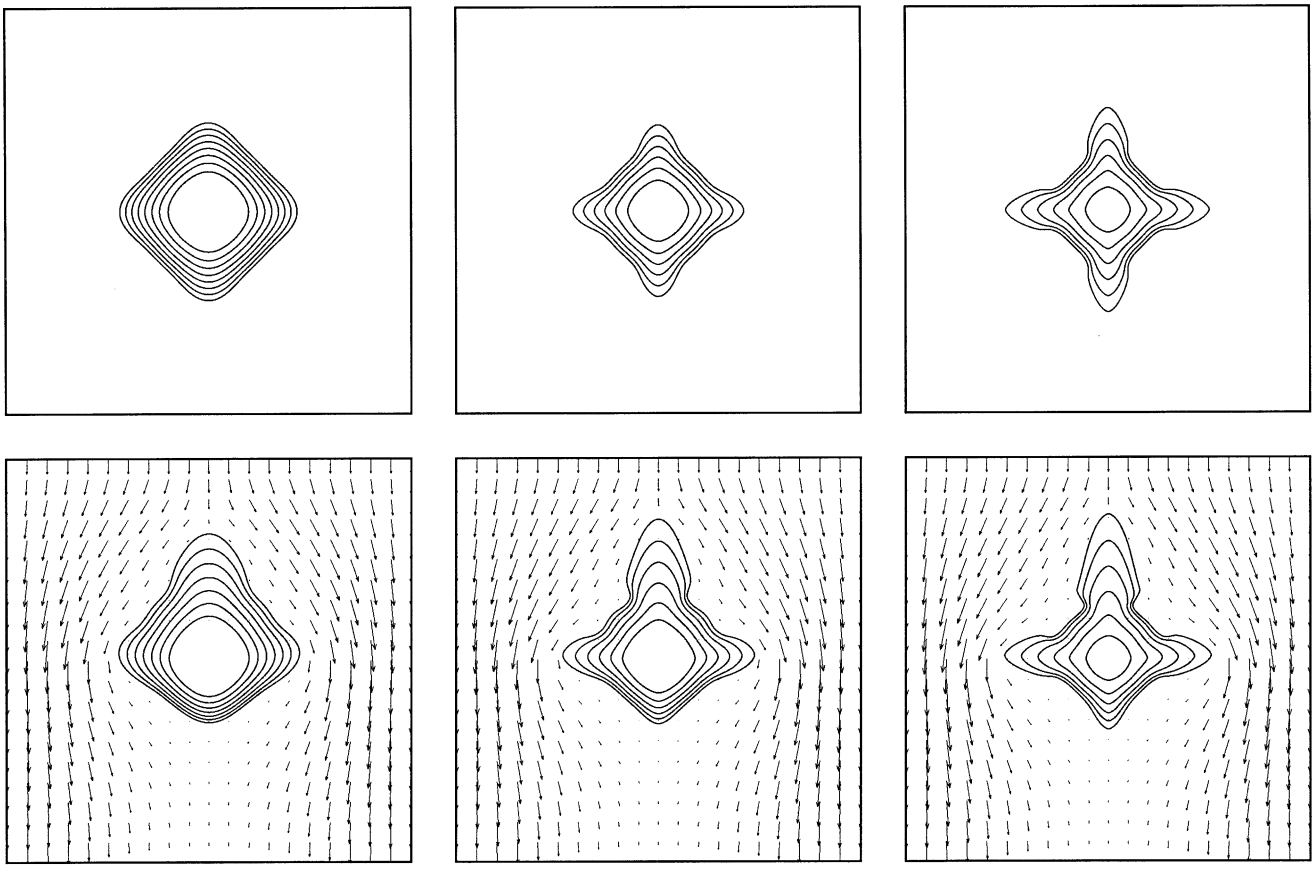

Fig. 6. Evolution of phase-filed contours for a dendrite. Upper panels: without convection; Lower panels: with convection; the anisotropy strengths are 0.01, 0.03, and 0.05 going from left to right.

coarsening of a dendrite. Combining Eqs. (7) and (8) yields:

$$\frac{\mathrm{d}F}{R\mathrm{d}U} = 1.75(Z/R)^{0.22} = 1.75\left(\frac{V_\mathrm{t}}{R}t\right)^{0.22}. \tag{9}$$

The exponent of 0.22 is not close to the classical coarsening exponent of 1/3, indicating that the overall coarsening of a side-branching dendrite cannot be explained by capillary-driven coarsening alone.

The parameter $\mathrm{d}F/\mathrm{d}U$ reflects the mean value of all curvatures in an axial section of a side-branching dendrite, including that from the primary stem. By removing the effect of the primary stem from $\mathrm{d}F/\mathrm{d}U$ it is possible to separately study the coarsening process of an individual side-branch during dendritic growth. To do this, the authors propose a mean side-branch radius, ρ_m, defined as:

$$\rho_\mathrm{m} = (\mathrm{d}F - \mathrm{d}F_\mathrm{ps})/(\mathrm{d}U - \mathrm{d}U_\mathrm{ps}), \tag{10}$$

where F_ps and U_ps are the projection area and the contour length of the primary stem. It can be seen from Fig. 2 that the quantity $(\Delta F - \Delta F_\mathrm{ps})/(\Delta U - \Delta U_\mathrm{ps})$ is actually an area-averaged radius of a side-branch if a branch is approximated as a cylindrical rod. Using measurement results for F_ps and U_ps [22]:

$$\rho_\mathrm{m}/R \approx 0.801(Z/R)^{0.341} = 0.0801(V_\mathrm{t}t/R)^{0.341} \quad \text{for } 40 < Z/R < 200, \tag{11}$$

which can be approximated and rewritten as:

$$\rho_\mathrm{m}^3 = 0.572(R^2V_\mathrm{t})t = 0.572(2\alpha_1 d_0/\sigma)t = 57.2\alpha_1 d_0 t \tag{12}$$

Compared with classical LSW theory, which describes the coarsening behavior of spherical particles in the limit of zero volume fraction solid as $\bar{\rho}^3(t) - \bar{\rho}_0^3 = \frac{8}{9}\alpha_1 d_0 t$, where $\bar{\rho}_0$ is the initial mean particle radius, the above result shows the same coarsening exponent of 1/3, but a much larger coarsening rate constant. Such a large rate constant cannot be explained using available theories for isothermal two-phase coarsening at a finite solid fraction. A reason for the discrepancy could be that the side-branches on a free dendrite have close neighbors only in the Z direction, while they are surrounded by supercooled melt in the circumferential direction and in the tip region. In particular, in the tip region of the active (or growing) side-branches, coarsening is controlled by heat transfer between the interface and the supercooled melt (net solidification) and competitive growth. Hence, the overall side-branch coarsening

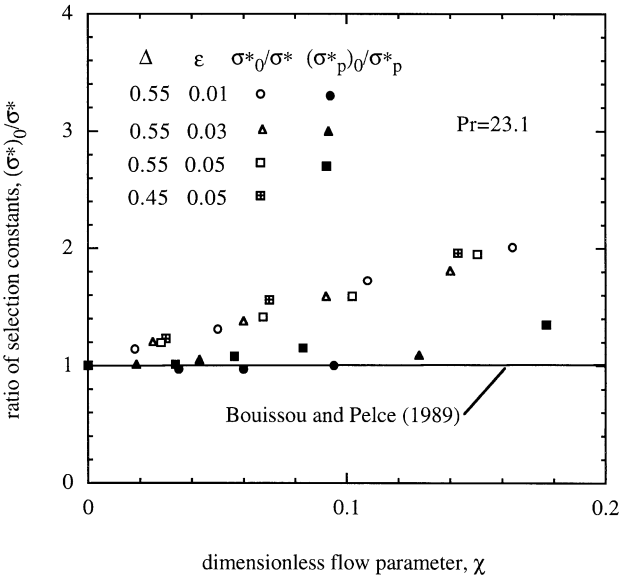

Fig. 7. Variation of the ratio of the selection constants without and with flow from the phase-flied simulations as a function the dimensionless flow parameter χ, and comparison with the solvability theory of Bouissou and Pelcé [26] (the theoretical lines for all three anisotropy strengths coincide); results are shown for the actual tip radius (open symbols) and the radius based on a parabolic fit (solid symbols).

process in free dendritic growth is driven by the combined effects of net solidification and interfacial energy reduction. Interestingly, the measured coarsening exponent shows excellent agreement with theories of purely capillary-driven coarsening. Only a more complete analysis of non-isothermal coarsening, with net solidification, can clarify this matter.

3. Phase-field simulation

The present phase-field simulation of dendritic growth with melt convection is directly based on the formulation of Karma and Rappel [21]. The heat, mass, and momentum conservation equations are derived using a volume averaging approach [24]. By including phase-field variable dependent advection terms in the conservation equations, the method addresses in a physically realistic way the transport of mass, momentum, heat, and solute by the 'residual' flow in the diffuse interface region. In this paper the authors only present some of the results obtained by using this method for the simulation of equiaxed dendritic solidification with melt flow. A description of the method can be found in Ref. [24] whilst a more detailed discussion of all results is available in Ref. [25].

Fig. 6 shows computed evolutions of equiaxed dendrites, growing at a fixed dimensionless supercooling of $\Delta = 0.55$, for three different anisotropy strengths ($\epsilon = 0.01$, 0.03 and 0.05) without flow (top panels) and with flow (bottom panels). For the bottom panels, the melt flows from the top to the bottom with a uniform inlet velocity of $Ud_0/\alpha_1 = 0.07$ and the Prandtl number is $Pr = \nu/\alpha_1 = 23.1$. It can be seen that in the presence of flow the dendrite acquires a highly asymmetric shape, with the upper tip growing much faster than the lower and horizontal tips. The flow causes much higher temperature gradients near the upper tip than near the lower tip. Another interesting observation is that the horizontal tips grow slightly upwards. This dendrite 'tilting' is due to the asymmetry of the heat fluxes on the sides of the horizontal branch. In the following the detailed morphological features of the dendrite are investigated through an examination of the tip operating state and the side-branching behavior.

3.1. Tip operating state

The operating state of a growing dendrite consists of the steady-state tip velocity V_t and radius R which are uniquely selected by the system under given growth conditions. Here, the effects of melt convection on the tip operating state, by measuring tip velocities and radii from the present simulations, are evaluated.

Tip velocity and radius measurements are carried out on all three tips (upstream, normal to flow, and downstream). It is found that while the upstream tip reaches a steady velocity, the horizontal and downstream tips continue to slightly slow down due to the ever increasing size of the dendrite relative to the domain. Nonetheless, approximate steady values of V_t and R can be measured for each tip. The knowledge of the tip radius and tip speed allows for the calculation of the selection constant, σ^*, as defined in $V_t R^2 \equiv 2d_0\alpha_1/\sigma^*$. As an example, for $\Delta = 0.55$, $\epsilon = 0.03$, $Ud_0/\alpha_1 = 0.135$ and $Pr = 23.1$, it is found that $\sigma^* \approx 0.31$ for the steady-state upstream tip, $\sigma^* \approx 0.36$ for the tip normal to flow, and $\sigma^* \approx 0.38$ for the downstream tip. For the corresponding pure diffusion case, it is found that $\sigma^* \approx 0.38$. The difference between the value of σ^* for the upstream tip and the no-flow tip suggests a significant influence of melt flow on the stability constant. This issue is investigated in more detail in the following by comparing the present results to the solvability theory of Bouissou and Pelcé [26] for dendrite tip growth with a uniform flow approaching from a direction opposite to the growth direction.

Bouissou and Pelcé [26] present a solvability theory that allows the selection constant σ^* to be predicted for the upstream tip in the presence of flow. The main result of this theory is that the ratio of the selection constant without flow, $(\sigma^*)_0$, to the value with flow, σ^*, is a function of a dimensionless parameter χ according to Ref. [26]:

$$\frac{(\sigma^*)_0}{\sigma^*} = 1 + f[\chi = a(Re)d_0U/(\beta^{3/4}RV_t)], \tag{13}$$

where f is a function, $\beta = 15\epsilon$, and:

$$a(Re) = \left(\frac{2Re}{\pi}\right)^{1/2} \frac{\exp(-Re/2)}{\mathrm{erfc}(\sqrt{Re/2})}, \tag{14}$$

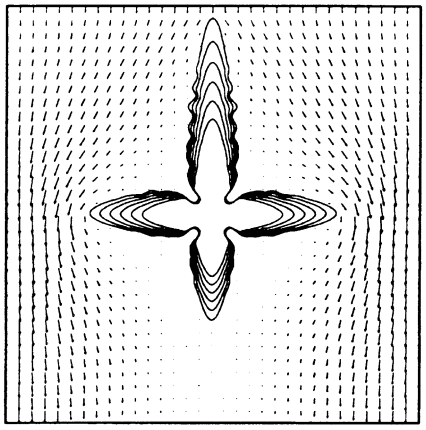

Fig. 8. Evolution of phase-flied contour for a side branching dendrite in the presence of flow.

in which $Re \equiv UR/\nu$ is the Reynolds number. Note that the parameter χ contains not only the flow velocity but also the anisotropy strength. For small χ, as is the case in the present simulations, Bouissou and Pelcé found that $f(\chi) \approx 0$, implying that the selection constant is independent of the flow velocity; for χ greater than about 30, $f(\chi) = b\chi^{11/14}$, where b is a constant. Fig. 7 shows a comparison of the σ^* ratios determined from the present simulations with Eqs. (13) and (14). The authors [25] determined the function f by solving numerically the complex solvability integral provided in Ref. [26]. It can be seen that the simulation σ^* ratios can be significantly above unity and increase strongly with increasing χ. This result is not in agreement with Eqs. (13) and (14), which show that the σ^* ratio remains very close to unity for the low χ values achieved in the present simulations. The disagreement can be explained by the strong variation of the solid/liquid interface curvature very near the tip and the deviation of the tip shape from a parabola especially for large anisotropy strengths.

By evaluating the local curvature of the interface from the phase-field predictions as a function of the distance, Z, from the dendrite tip, it was found that the deviation from a parabolic shape is limited to a distance no larger than about one tip radius. The authors then fitted a parabola to the predicted interface in the region away from the tip, and determined the tip radius, R_p, from this parabolic fit. Note that ρ_p is likely to be the tip radius measured in experiments. The σ^* ratios, $(\sigma_p^*)_0/\sigma_p^*$, based on the parabolic fit radius, instead of the actual tip radius, are also shown in Fig. 7. It can be seen that they remain close to unity, even though the tip velocities vary by several hundred percent. The good agreement with the theory of Bouissou and Pelcé, Eqs. (13) and (14), indicates that within the parabolic tip shape approximation the present simulations provide the correct tip velocity selection.

3.2. Side-branching behavior

By incorporating a thermal noise source term into the energy equation used in the phase-field method, Karma and Rappel [27] recently studied the initial stage of side-branch formation during dendritic growth without flow. Their calculation of the side-branching characteristics (root-mean-square amplitude and mean side-branch spacing) shows good agreement with analytical predictions based on linear theory of noise amplification [8,10].

The evolution of the side-branching in dendritic growth with flow is illustrated in Fig. 8. The figure shows the effect of the orientation of a growing branch with respect to the flow on the side-branching behavior. Among the four branches of an equiaxed dendrite the upstream branch is the only one where the formation and development of side-branches is observed. A comparison with the corresponding pure diffusion case indicates that while the development of side-branches on the upstream branch is apparently promoted by melt flow, the side-branching phenomenon on the other branches (downstream or normal to the flow) seems to be suppressed by this flow. The systematic measurement of the side-branch spacings and the mean side-branch amplitude are in progress and will quantify the effects of the melt flow on the microstructural evolution in equiaxed dendritic solidification.

4. Conclusions

The recent work of the authors in the understanding and modeling of microstructure evolution in equiaxed dendritic growth is reviewed. The work involves both experimental measurements and numerical simulations. Measurements are performed on freely growing SCN dendrited using images from the microgravity experiment of Glicksman and co-workers and focus on the side-branching behavior. The results reveal unique scaling relations between the geometry parameters of side-branching dendrites and the steady-state primary tip radius. Two different regimes in the side-branching evolution, an initial linear regime and a subsequent non-linear coarsening regime are found. A simple model, based on the Mullins–Sekerka linear stability theory, is developed to describe the initial side-branching behavior and is found to be in excellent agreement with the experimentally measured arm spacings, indicating that the initial side-branch spacings are selected by the maximum instability wavelength. In the non-linear regime, it is found that the conventional measurements of individual side-branches, such as the spacing or the length or side-branches, can only reveal part of the coarsening process. A mean side-branch radius, which is derived from measurements of integral parameters, is proposed to characterize the overall coarsening process of an individual side-branch during free dendritic growth. While its coarsening behavior follows the classical cube root of time law, the large coarsening rate constant suggests that new theories of non-isothermal coarsening need to be developed to explain the measurements completely.

Regarding the modeling work, a phase-field model is presented for the direct numerical simulation of microstructural evolution in dendritic growth with melt flow. The dendrite tip velocities, radii, and selection criterion in the presence of flow are evaluated. It is found that depending on the tip growth direction with respect to the flow the tip radii and velocities can be either above or below the values for pure heat diffusion. For the upstream tip, the simulated selection constants are in agreement with the Microscopic Solvability Theory with flow of Boussou and Pelcé [26], if the tip radius is based on a parabolic fit of the predicted dendrite shape away from the tip. If the actual tip radius is used, however, the finite crystalline anisotropy causes significant deviations of the simulation results from the theory. Introducing noise into the simulation, the authors also investigated the side-branch formation in the presence of melt flow. The preliminary results show that, depending on the direction of the flow; the development of side-branches can be either promoted or suppressed. A quantitative evaluation of the predicted side-branch structure in the presence of melt flow is presently underway. Extension of the simulations to three dimensions and lower supercoolings will ultimately allow for direct comparisons with the experimental measurements reviewed in the first part of this article.

Acknowledgements

This work was supported by, NASA under contract NCC8-94. The authors are indebted to Professor Glicksman of RPI and NASA for making the IDGE images available to them.

References

[1] J.S. Langer, Science 243 (1989) 1150.
[2] Y. Pomeau, M. Ben Amar, in: C. Godreche (Ed.), Solids Far From Equilibrium, Cambridge University Press, Cambridge, 1992.
[3] D. Kessler, J. Koplik, H. Levine, Adv. Phys. 37 (1988) 255.
[4] S.C. Huang, M.E. Glicksman, Acta Metall. 29 (1981) 701–717.
[5] M.E. Glicksman, M.B. Koss, E.A. Winsa, Phys. Rev. Lett. 73 (1993) 573.
[6] W.W. Mullins, R.F. Sekerka, J. Appl. Phys. 35 (1964) 444.
[7] R. Pieters, J.S. Langer, Phys. Rev. Lett. 56 (1986) 1948.
[8] J.S. Langer, Phys. Rev. A 36 (1987) 3350.
[9] M.N. Barber, A. Barbieri, J.S. Langer, Phys. Rev. A 36 (1987) 3340.
[10] E. Brener, D. Temkin, Phys. Rev. E 51 (1995) 351.
[11] E. Brener, Phys. Rev Lett. 71 (1993) 3653.
[12] U. Bisang, J.H. Bilgram, Phys. Rev. Lett. 75 (1995) 3898.
[13] U. Bisang, J.H. Bilgram, Phys. Rev. E 54 (1996) 5309.
[14] J.C. LaCombe, M.B. Koss, V.E. Fradkov, M.E. Glicksman, Phys. Rev. E 52 (1995) 2778.
[15] E. Hürlimann, R. Trittibach, U. Bisang, J.H. Bilgram, Phys. Rev. A 46 (1992) 6579.
[16] A. Dougherty, R. Chen, Phys. Rev. A 46 (1992) R4508.
[17] Q. Li, C. Beckermann, Phys. Rev. E 57 (1988) 3176.
[18] G. Caginalp, in: L. Garrido (Ed.), Application of Field Theory to Statistical Mechanics, Springer, Berlin, 1985, p. 216.
[19] A.A. Wheeler, W.J. Boettinger, G.B. McFadden, Phys. Rev. A 45 (1992) 7424.
[20] R. Kobayashi, Physica D 63 (1993) 410.
[21] A. Karma, W.-J. Rappel, Phys. Rev. E 57 (1998) 4323.
[22] Q. Li, C. Beckermann, Acta Mater. 47 (1999) 2345.
[23] Y. Couder, F. Argoul, A. Arneodo, J. Maurer, M. Rabud, Phys. Rev. A 42 (1990) 3499.
[24] C. Beckermann, H.-J. Diepers, I. Steinbach, A. Karma, X. Tong, J. Comp. Phys. 154 (1999) 468.
[25] X. Tong, C. Beckermann, A. Karma, Phys. Rev. E 61 (2000) R49.
[26] P. Bouissou, P. Pelcé, Phys. Rev. A 40 (1989) 6673.
[27] A. Karma, W.-J. Rappel, Phys. Rev. E 60 (1999) 3614.